Inorganic Chemistry

Article

pubs.acs.org/IC

Oxidatively Induced Reactivity of $[Fe_2(CO)_4(\kappa^2\text{-dppe})(\mu\text{-pdt})]$: an Electrochemical and Theoretical Study of the Structure Change and Ligand Binding Processes

Dounia Chouffai,[†] Giuseppe Zampella,*[,‡] Jean-François Capon,[†] Luca De Gioia,*[,‡] Frédéric Gloaguen,[†] François Y. Pétillon,[†] Philippe Schollhammer,*[,†] and Jean Talarmin*

[†]UMR CNRS 6521, Chimie, Electrochimie Moléculaires et Chimie Analytique, Université de Bretagne Occidentale, UFR Sciences et Techniques, Cs 93837, 29238 Brest-Cedex 3, France

[‡]Department of Biotechnology and Bioscience, University of Milano-Bicocca, Piazza della Scienza 2, 20126 Milan, Italy

Supporting Information

ABSTRACT: The one-electron oxidation of the diiron complex $[Fe_2(CO)_4(\kappa^2\text{-dppe})(\mu\text{-pdt})]$ (**1**) (dppe = $Ph_2PCH_2CH_2PPh_2$; pdt = $S(CH_2)_3S$) has been investigated in the absence and in the presence of $P(OMe)_3$, by both electrochemical and theoretical methods, to shed light on the mechanism and the location of the oxidatively induced structure change. While cyclic voltammetric experiments did not allow to discriminate between a two-step (EC) and a concerted, quasi-reversible (QR) process, density functional theory (DFT) calculations favor the first option. When $P(OMe)_3$ is present, the one-electron oxidation produces singly and doubly substituted cations, $[Fe_2(CO)_{4-n}\{P(OMe)_3\}_n(\kappa^2\text{-dppe})(\mu\text{-pdt})]^+$ (n = 1: $\mathbf{2}^+$; n = 2: $\mathbf{3}^+$) following mechanisms that were investigated in detail by DFT. Although the most stable isomer of $\mathbf{1}^+$ and $\mathbf{2}^+$ (and $\mathbf{3}^+$) show a rotated Fe(dppe) center, binding of $P(OMe)_3$ occurs at the neighboring iron center of both $\mathbf{1}^+$ and $\mathbf{2}^+$. The neutral compound **3** was obtained by controlled-potential reduction of the corresponding cation, while **2** was quantitatively produced by reaction of **3** with CO. The CO dependent conversion of **3** into **2** as well as the $\mathbf{2}^+ \leftrightarrow \mathbf{3}^+$ interconversion were examined by DFT.

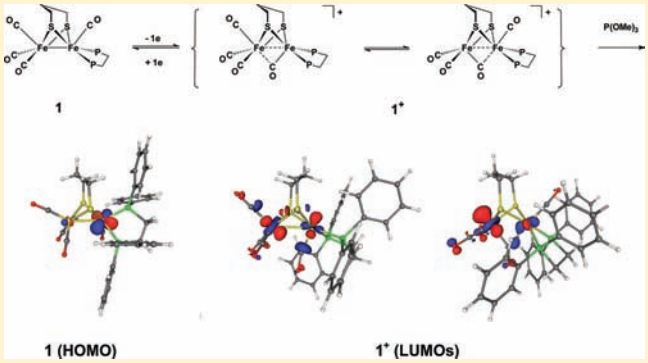

INTRODUCTION

One obvious difference between the active site of [FeFe]-hydrogenases, the H-cluster, and the synthetic compounds of general formula $[Fe_2(CO)_{6-x}(L)_x(\mu\text{-dithiolate})]$ is the geometry of the diiron core, where the pyramids about the metal centers are eclipsed (Fe(I)Fe(I) models) rather than inverted with a bridging or semibridging carbonyl (enzymes) (Scheme 1).[1−3] A consequence of this structural difference is to promote the formation of a bridging hydride upon protonation of most of the models,[4] which is less effective toward formation of H_2 than the terminal hydride[5] probably formed at the enzyme active site.[3,6−8]

Scheme 1. Schematic Representation of the Active Site of the [FeFe]H_2ases (H-cluster) and of Model Compounds in the Eclipsed and Rotated Geometry

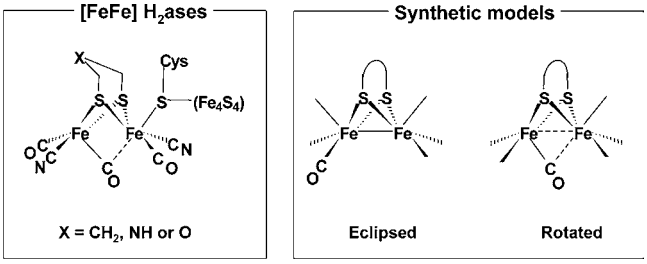

Recent research has been undertaken to identify the factors that would favor the inverted geometry found at the enzymes' diiron subsite, the so-called rotated state. Theoretical calculations showed that one of these factors is a dissymmetric substitution at the iron centers,[9] which stimulated the synthesis of model compounds bearing chelating ligands. Although crystallographic data proved that the $[Fe_2(CO)_4(\kappa^2\text{-LL})(\mu\text{-dithiolate})]$ models still adopted an eclipsed geometry in the solid,[10−15] some aspects of their chemistry,[13] and particularly the transient formation of terminal hydrides upon protonation[10d,14] suggested an easier access to the rotated state than in the symmetrically disubstituted analogues.

A few years ago, a Fe(I)Fe(II) complex with both a coordination sphere and spectroscopic properties similar to those of the CO-inhibited [FeFe]-hydrogenases[16] was obtained by oxidation of a Fe(I)Fe(I) precursor.[17] More recently, Fe(I)Fe(II) compounds with a rotated geometry were crystallographically

Received: July 26, 2011
Published: November 22, 2011

   dx.doi.org/10.1021/ic201601q | *Inorg. Chem.* 2011, 50, 12575−12585

characterized.[18−21] Detailed studies of the role of the bridging dithiolate and of the terminal ligands on the geometry about the iron centers in the Fe(I)Fe(II) oxidation state, and of the reactivity of the oxidized complexes with CO, were also reported.[19−25]

The oxidatively induced structure change, which may lend itself to electrochemical investigations,[26−32] generates an open coordination site in the apical position on the rotated iron center, whose reactivity with substrates may also be investigated by electrochemical means. The characterization of a complex resulting from the reaction of a substrate at this vacant site would also provide indirect evidence as to which of the iron centers underwent isomerization. In relation with these issues, we now report a combined electrochemical and density functional theory (DFT) investigation of the oxidation of a dissymmetrically disubstituted diiron complex, $[Fe_2(CO)_4(\kappa^2\text{-dppe})(\mu\text{-pdt})]$ (**1**),[14a] in the absence and in the presence of $P(OMe)_3$ (dppe = $Ph_2PCH_2CH_2PPh_2$; pdt = $S(CH_2)_3S$).

RESULTS

1. Oxidation of $[Fe_2(CO)_4(\kappa^2\text{-dppe})(\mu\text{-pdt})]$ (1). The cyclic voltammetry (CV) of $[Fe_2(CO)_4(\kappa^2\text{-dppe})(\mu\text{-pdt})]$ (**1**) shows that the complex undergoes two oxidations, the first of which is quasi-reversible with $E_{1/2}^{ox1} = -0.24 \pm 0.01$ V in CH_2Cl_2-$[NBu_4][PF_6]$.[33] The second, irreversible, oxidation ($E_p^{ox2} \sim 0.7$ V, Table 1) which gives rise to products detected by their reduction on the return scan ($E_p \sim 0$ and -0.5 V) (Figure 1) was not investigated.

Table 1. Redox Potentials of the Complexes in CH_2Cl_2-$[NBu_4][PF_6]$

complex	$E_{1/2}^{ox1}$ V/Fc	E_p^{ox2} V/Fc
$[Fe_2(CO)_4(\kappa^2\text{-dppe})(\mu\text{-pdt})]$ (**1**)	−0.24	0.68
$[Fe_2(CO)_3\{P(OMe)_3\}(\kappa^2\text{-dppe})(\mu\text{-pdt})]$ (**2**)	−0.54	0.5
$[Fe_2(CO)_2\{P(OMe)_3\}_2(\kappa^2\text{-dppe})(\mu\text{-pdt})]$ (**3**)	−0.88	0.14

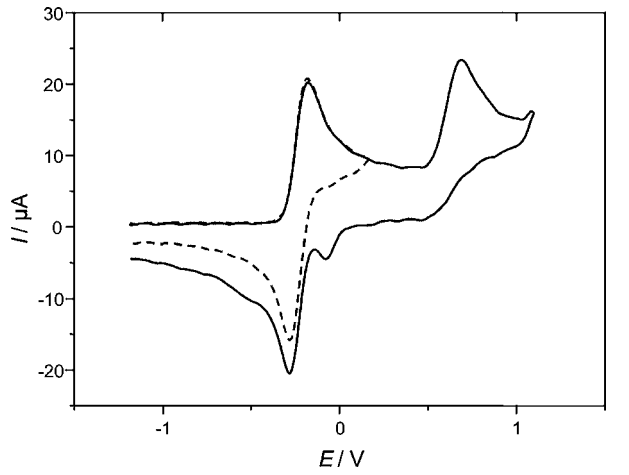

Figure 1. CV of $[Fe_2(CO)_4(\kappa^2\text{-dppe})(\mu\text{-pdt})]$ (**1**) (1.13 mM) in CH_2Cl_2-$[NBu_4][PF_6]$ (vitreous carbon electrode; $v = 0.2$ V s^{-1}; potentials are in V vs Fc^+/Fc).

The comparison of the current function $[i_p/v^{1/2}]$ for the first oxidation of **1** and for the one-electron oxidation of $[Fe_2(CO)_4(\kappa^2\text{-dppe})(\mu\text{-pdt})(\mu\text{-H})]^+$ (Supporting Information, Figure S1) shows that the former is also a one-electron process.[34] Controlled-potential electrolysis of a solution of **1** in CH_2Cl_2-$[NBu_4][PF_6]$ at room temperature yielded very low amounts of the expected cation ($E_{1/2}^{red} = -0.25$ V, $E_p^{ox} = 0.74$ V) along with unidentified products. Electrolysis of **1** carried out at −10 °C produced $\mathbf{1}^+$ almost quantitatively[40] after the transfer of 1 F mol^{-1} **1**. $\mathbf{1}^+$ was also obtained by chemical oxidation of **1** (1 equiv ferrocenium, −10 °C) in CH_2Cl_2. Both the redox potential of **1** and the infrared spectrum of $\mathbf{1}^+$ in CH_2Cl_2 (ν(CO) = 2079 (s), 2021 (s), 1920(w) cm^{-1}) are similar to those of the (κ^2-dppv) analogue (dppv = $Ph_2PCH{=}CHPPh_2$).[21]

Previous experimental and theoretical studies have demonstrated that one-electron oxidation of $[Fe_2(CO)_4(L)(L')(\mu\text{-dithiolate})]$ or $[Fe_2(CO)_4(\kappa^2\text{-LL})(\mu\text{-dithiolate})]$ complexes in which the geometry of the pyramids about the metal centers is eclipsed (**E**) resulted in a cation with a rotated structure ($\mathbf{R}^+$)[18−25,35] (Scheme 2). Structural changes induced by electrode reactions may occur according to different mechanisms, depending on whether the isomerization is concerted with the electron transfer (quasi-reversible process, along the diagonal in Scheme 2) or occurs as a following reaction (two-steps EC process, Scheme 2), which leads to a square scheme mechanism in case of chemical reversibility.

Scheme 2

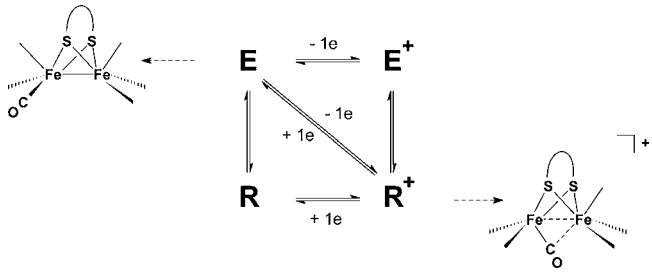

It is frequent that the only species detected by CV are the starting material **E** and the rearranged oxidized derivative $\mathbf{R}^+$ (in case of an oxidatively induced structure change, Scheme 2) which makes the distinction between the two mechanisms difficult.[27−29] Experimentally, the two possibilities may be distinguished if a supplementary redox event (reduction of $\mathbf{E}^+$ or oxidation of **R**, Scheme 2), proving the existence of a square scheme, is observable under specific conditions. However, that a supplementary redox step cannot be detected does not disprove the existence of a square scheme.[26−30,36]

Our experimental attempts to discriminate between the two possibilities failed. In the present case, CV at low temperature (−40 °C) only resulted in an increase of the anodic to cathodic peak separation (ΔE_p) compared to the CVs run at room temperature. CV at different scan rates (up to 40 V s^{-1}), that also lead to an increase of ΔE_p with increasing v, showed that the oxidation of **1** becomes broader when $v \geq 2$ V s^{-1}. A distinct shoulder was present around −0.07 V, while it was not observed at lower v. However, this is assigned to the separate oxidation of the two eclipsed isomers of **1** with basal-apical and dibasal binding of the dppe chelate that were identified by NMR spectroscopy,[14a] rather than to the oxidation of **1** in the eclipsed and rotated geometries.

Although an EC mechanism cannot be ruled out on the basis of the experimental results, we assumed the occurrence of a quasi-reversible process to work out the apparent heterogeneous electron transfer rate constant from the scan rate

dx.doi.org/10.1021/ic201601q | Inorg. Chem. 2011, 50, 12575−12585

dependence of ΔE_p.[37] Digital simulations[38] of the electrochemical oxidation of **1** were also carried out according to the quasi-reversible scheme. A comparison of the experimental and simulated CVs is presented as Supporting Information (Supporting Information, Figure S2). The agreement is reasonable at slow scan rates, the difference noted at faster scan rates is assigned to the fact that a single isomer of **1** was considered in the simulations.

To complement the experimental investigation on the mechanism of the oxidation of $[Fe_2(CO)_4(\kappa^2\text{-dppe})(\mu\text{-pdt})]$ (**1**), DFT calculations were carried out to characterize the stereoelectronic properties of **1** and $\mathbf{1}^+$. It turned out that the minimum energy conformation of **1** corresponds to an eclipsed form featuring basal-apical dppe, in agreement with experimental results. As for $\mathbf{1}^+$, the lowest energy isomer corresponds to a structure characterized by rotation of the Fe(dppe) moiety (Figure 2). Also an eclipsed $\mathbf{1}^+$ isomer closely resembling the

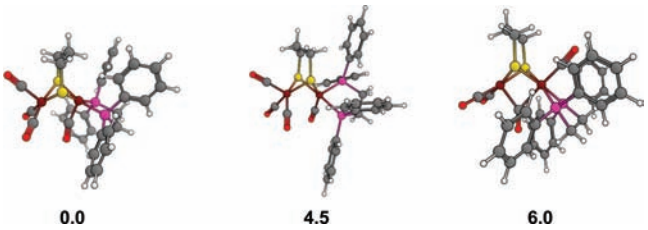

Figure 2. DFT optimized structures of relevant $\mathbf{1}^+$ isomers. The energy (in kcal/mol) of each isomer, relative to the lowest-energy one, is shown below each structure. For the sake of clarity atoms are shown as follow. Carbon, gray; hydrogen, white; sulfur, yellow; oxygen, red; phosphorus, light purple; iron, dark purple.

structure of the parent compound **1** (i.e., basal-apical dppe) corresponds to an energy minimum. However, the energy of the eclipsed $\mathbf{1}^+$ form is 4.5 kcal/mol higher than for the rotated isomer. Another rotated $\mathbf{1}^+$ isomer, featuring rotation of the $Fe(CO)_3$ moiety, is 6.0 kcal/mol higher in energy (Figure 2). Other $\mathbf{1}^+$ isomers are even higher in energy (data not shown).

2. Oxidation of $[Fe_2(CO)_4(\kappa^2\text{-dppe})(\mu\text{-pdt})]$ (1) in the Presence of $P(OMe)_3$ and Characterization of $[Fe_2(CO)_{4-n}\{P(OMe)_3\}_n(\kappa^2\text{-dppe})(\mu\text{-pdt})]$ (n = 1, (2); n = 2, (3)). The CV of **1** in CH_2Cl_2-$[NBu_4][PF_6]$ at room temperature shows that the oxidation peak current is little affected by the presence of $P(OMe)_3$ while the chemical reversibility of the $\mathbf{1}^{0/+}$ couple is scan rate dependent, which demonstrates the occurrence of an EC process.[33,39] The product of the follow-up reaction(s) is detected by a reversible reduction at −0.54 V (Figure 3) and an irreversible oxidation at 0.5 V (not shown in Figure 3).

Electrosyntheses were carried out to isolate (see below) the product of the reaction of $\mathbf{1}^+$ with $P(OMe)_3$. Controlled-potential oxidation of a CH_2Cl_2-$[NBu_4][PF_6]$ solution of **1** in the presence of 1 equiv of $P(OMe)_3$ at room temperature (E_{el} = −0.2 V, graphite anode) was completed after the passage of about 0.9 F mol^{-1} **1**. CV of the electrolyzed solution showed that the expected product, with $E_{1/2}^{red}$ = −0.54 V and E_p^{ox} = 0.5 V, was accompanied by a second one, with $E_{1/2}^{red}$ = −0.88 V and E_p^{ox} = 0.14 V. Thus, reactions that are too slow for detection by CV generated the latter on the longer time scale of electrolysis. Electrolyses performed in the presence of larger amounts of $P(OMe)_3$ (2−4 equiv) resulted in the almost quantitative formation[40] of the second product ($\mathbf{3}^+$), that was barely detected by CV before electrolysis (Figure 4). A reverse

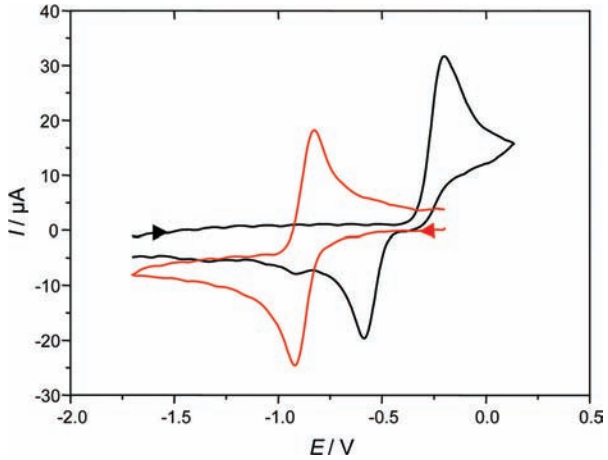

Figure 4. CV of $[Fe_2(CO)_4(\kappa^2\text{-dppe})(\mu\text{-pdt})]$ (**1**) (1.2 mM) in the presence of 3 equiv of $P(OMe)_3$ before (black lines) and after (red lines) controlled-potential electrolysis at room temperature (E_{el} = −0.2 V; 0.9 F mol^{-1} **1**) (CH_2Cl_2-$[NBu_4][PF_6]$; ν = 0.2 V s^{-1}; vitreous carbon electrode; potentials are in V vs Fc^+/Fc).

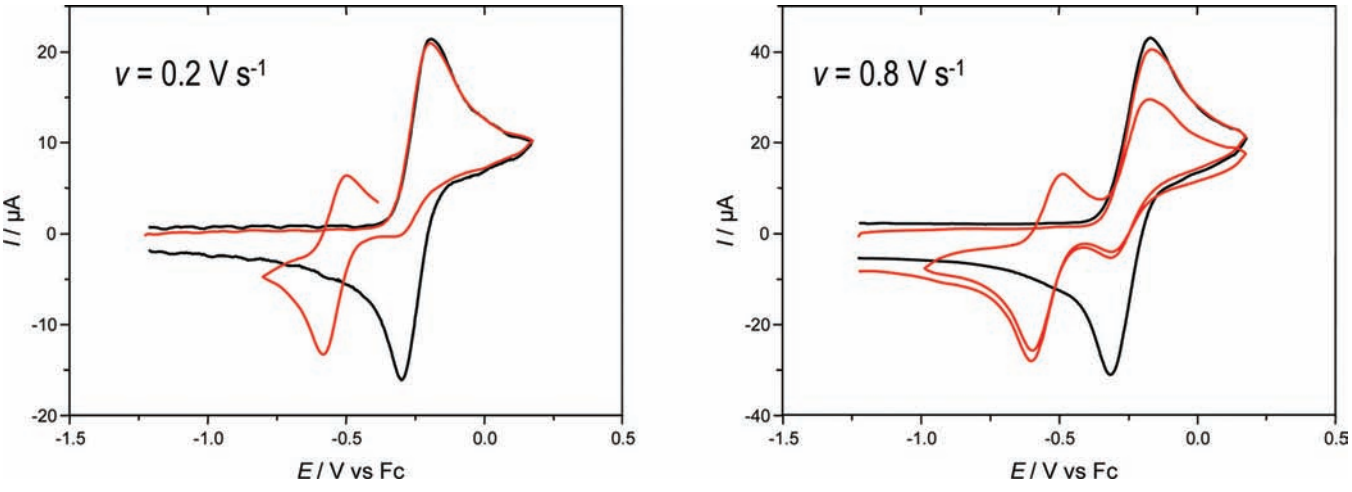

Figure 3. CV of $[Fe_2(CO)_4(\kappa^2\text{-dppe})(\mu\text{-pdt})]$ (**1**) (1.1 mM) in CH_2Cl_2-$[NBu_4][PF_6]$ in the absence (black lines) and in the presence (red lines) of 1 equiv of $P(OMe)_3$ (vitreous carbon electrode; potentials are in V vs Fc^+/Fc).

dx.doi.org/10.1021/ic201601q | Inorg. Chem. 2011, 50, 12575−12585

electrolysis at −0.96 V generated a brown solution of the corresponding neutral complex after the transfer of about 0.9 F mol^{-1} of the initial **1** (Supporting Information, Figure S8). The neutral species, obtained in >80% yield,[40] was identified as $[Fe_2(CO)_2\{P(OMe)_3\}_2(\kappa^2\text{-dppe})(\mu\text{-pdt})]$ (**3**) on the basis of IR and NMR spectroscopies and indirectly by its reactivity toward CO which gives $[Fe_2(CO)_3\{P(OMe)_3\}(\kappa^2\text{-dppe})(\mu\text{-pdt})]$ (**2**). The redox potential of the $\mathbf{3}^{0/+}$ couple (Table 1) and the infrared spectra of **3** (ν(CO) in CH_2Cl_2 = 1899 (s), 1880 (s) cm^{-1}) and $\mathbf{3}^+$ (ν(CO) in CH_2Cl_2 = 1962 (s), 1887 (w) cm^{-1}) are similar to those of $[Fe_2(CO)_2(\kappa^2\text{-dppv})_2(\mu\text{-xdt})]^{0/+}$ (xdt = pdt or edt; edt = SCH_2CH_2S).[22,41] Satisfactory ^{1}H NMR data of **3** could not be obtained, but the ^{31}P-{^{1}H} NMR spectrum of **3** in $CDCl_3$, displays two singlets at 177.5 ppm and 85.4 ppm, which are assigned unambiguously to the trimethylphosphite[42] and to the chelated diphosphine[43] ligands, respectively. Variable-temperature ^{31}P-{^{1}H} NMR experiments revealed that **3** is fluxional. Several dynamic processes related to the dppe, $P(OMe)_3$ or μ-pdt groups may be operative in solution and this makes the determination of the nature and the number of isomers difficult to state unambiguously. (see Supporting Information, Figure S3).

The singly $P(OMe)_3$-substituted analogue, $[Fe_2(CO)_3\{P(OMe)_3\}(\kappa^2\text{-dppe})(\mu\text{-pdt})]$ (**2**), was obtained by bubbling CO through the solution of **3**. **3** was not recovered upon flushing the CO-saturated solution with N_2. X-ray analysis of a single crystal of **2**, obtained from dichloromethane-hexane (1:1) mixture at −18 °C, established without any ambiguity the structure, in solid state, of **2** with a basal-apical binding mode of the diphosphine group and an apical position of the $P(OMe)_3$ ligand (Figure 5). **2** is structurally analogous to other

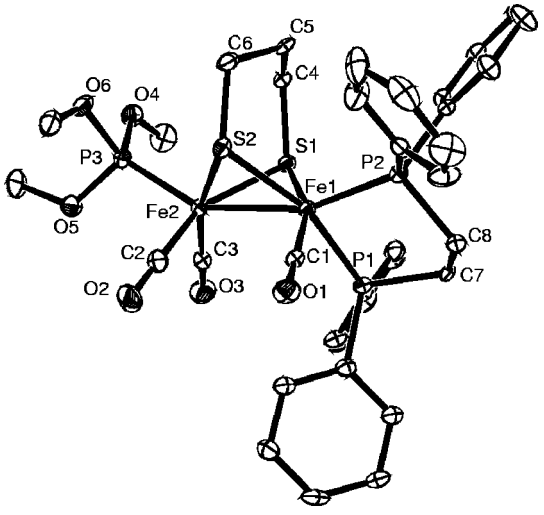

Figure 5. Structure of $\mathbf{2}\cdot CH_2Cl_2,C_6H_{14}$ showing 30% thermal ellipsoids (CH_2Cl_2 and C_6H_{14} are omitted for clarity). Selected distances (Å) and angles (deg): Fe1−Fe2, 2.5474(13), P1−Fe1, 2.217(2), P2−Fe1, 2.199(2), P3−Fe2, 2.155(2), S1−Fe2, 2.2699(19), S1−Fe1, 2.2728(19), S2−Fe1, 2.2626(19), S2−Fe2, 2.269(2), P2−Fe1−P1, 88.05(7), Fe2−S1−Fe1, 68.22(6), Fe1−S2−Fe2, 68.40(6).

trisubstituted diiron complexes of general formula $[Fe_2(CO)_3L(\kappa^2\text{-chelate})(\mu\text{-dithiolate})]$.[44,45]

2 was also characterized by elemental analyses and IR and NMR spectroscopies. The IR spectrum of **2** in dichloromethane displays three ν(CO) bands at 1968(s), 1913(s), and 1892(sh) cm^{-1}. Two singlets are observed at 179.7 (1 P) and 89.4 ppm (2 P) in the ^{31}P-{^{1}H} NMR spectrum in CD_2Cl_2 and assigned to $P(OMe)_3$ and dppe ligands, respectively. The ^{1}H NMR spectrum displays the set of resonances expected for trimethylphosphite, dppe and pdt groups (see Experimental Section). A VT ^{31}P-{^{1}H} NMR experiment, in CD_2Cl_2, revealed that **2** is fluxional. At −90 °C in CD_2Cl_2, two signals are observed in the phosphite region as well as three resonances for the phosphorus atoms of the diphosphine (see Supporting Information, Figure S4). These observations suggest that two isomers differing at least by the binding mode of the diphosphine are present in solution in a ratio close to 1:1. One of them is characterized by a singlet, at 94.1 ppm, that could be assigned to two equivalent phosphorus atoms of a symmetrically bonded dibasal dppe ligand with the phosphite lying in an apical orientation. The other two signals at 90.1 and 94.5 ppm could be attributed to two inequivalent phosphorus atoms of a basal-apical dppe group of the second isomer. This would be consistent with the results of the X-ray diffraction study.

Attempts to synthesize **2** by replacing one carbonyl group by $P(OMe)_3$ in **1** in refluxing toluene gave a mixture of **2** (minor product) and of a disubstituted compound **4**, having a pendant dppe ligand, $[Fe_2(CO)_4\{P(OMe)_3\}(\kappa^1\text{-dppe})(\mu\text{-pdt})]$ (**4**), in a ratio about 1:10 (see Supporting Information, Figure S5). Such a CO-migration in the ligand substitution process has already been reported for an analogous $[Fe_2(CO)_4(\kappa^2\text{-PNP})(\mu\text{-pdt})]$ compound (PNP = $(EtO)_2PN(Me)P(EtO)_2$).[46] The reaction producing **4** was not studied further. The reaction of **2** with $HBF_4\cdot OEt_2$ was also monitored by VT ^{1}H NMR spectroscopy. The protonation process is similar to that reported for $[Fe_2(CO)_3\{PMe_3\}(\kappa^2\text{-dppv})(\mu\text{-pdt})]$.[47] The initial formation of a transient terminal hydride species at low temperature and its isomerization upon warming into, successively, three bridging hydride forms with different phosphite and diphosphine positions, are observed (see Supporting Information, Figure S6).

Complex **2** undergoes a quasi-reversible oxidation at $E_{1/2}$ = −0.54 V (Figure 6a, red trace, Table 1) indicating that $\mathbf{2}^+$, formed along the reactions in Scheme 3, is the product detected by CV before electrolysis (Figure 2). Digital simulations[38] of the EC process in Scheme 3 are in fair agreement with the experimental CVs (Supporting Information, Figure S7).

The presence of $\mathbf{3}^+$ after controlled-potential electrolysis is in accord with its formation from $\mathbf{2}^+$ and $P(OMe)_3$ (Supporting Information, Figure S9). In a way similar to the CO-induced conversion of **3** to **2** (Figure 6a), complex $\mathbf{3}^+$ reacts with CO to generate $\mathbf{2}^+$ (Figure 6b). However, the reaction is at equilibrium ($\mathbf{2}^+/\mathbf{3}^+$: 1.2/1) and appears more complicated than a mere substitution of $P(OMe)_3$ by CO. The occurrence of a minor homogeneous redox process is indicated by the presence of a small irreversible oxidation peak at the same potential as the oxidation of **1** [that is irreversible in the presence of $P(OMe)_3$] (Figure 6b, red trace). This peak, as well as a small reduction at the same potential as the $\mathbf{2}^{+/0}$ couple, are still observed after flushing the solution with N_2 for a prolonged period (Figure 6b, blue trace). The presence of **1** is proposed to arise from the disproportionation of a species formed in low concentration under the present experimental conditions, by reaction of $\mathbf{3}^+$ with CO (see Discussion).

3. DFT Investigations of the Reactivity of $\mathbf{1}^+$ and $\mathbf{2}^+$ with $P(OMe)_3$. To shed further light on the reactivity of $\mathbf{1}^+$, we have used DFT to dissect the reaction mechanism for the

dx.doi.org/10.1021/ic201601q | Inorg. Chem. 2011, 50, 12575−12585

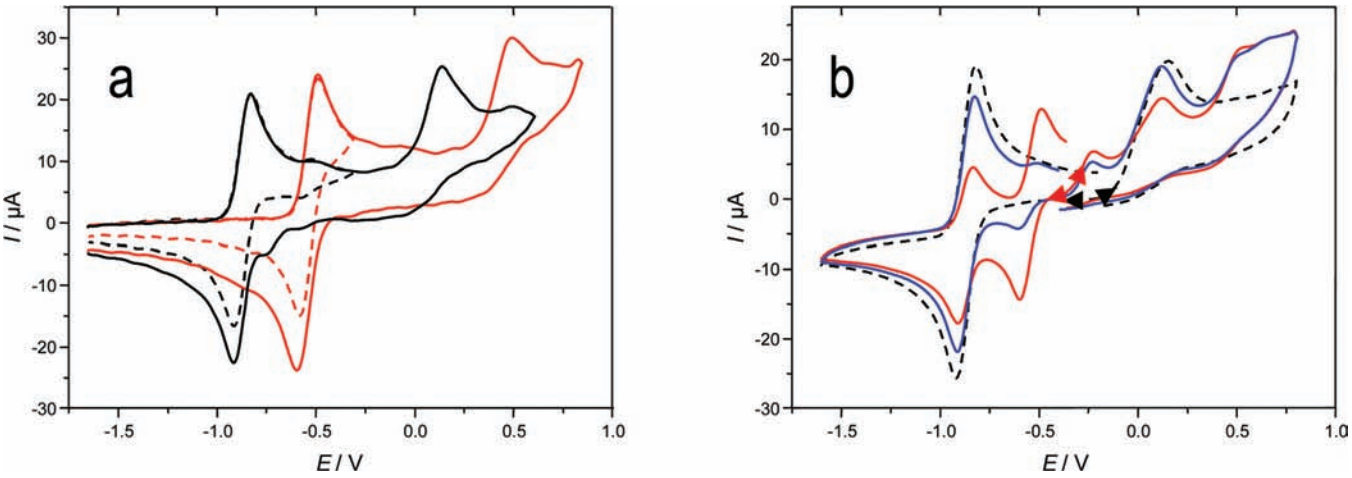

Figure 6. (a) CV of $[Fe_2(CO)_2\{P(OMe)_3\}_2(\kappa^2\text{-dppe})(\mu\text{-pdt})]$ (**3**) in CH_2Cl_2-$[NBu_4][PF_6]$ before (black lines) and after (red lines) bubbling CO through the solution (which generates **2**); (b) CV of $[Fe_2(CO)_2\{P(OMe)_3\}_2(\kappa^2\text{-dppe})(\mu\text{-pdt})]^+$ ($\mathbf{3}^+$) in CH_2Cl_2-$[NBu_4][PF_6]$ before (dashed lines) and after (red lines) bubbling CO through the solution, and after flushing the solution with N_2 (blue lines); the start potential and scan directions are the same for the red and blue traces (ν = 0.2 V s^{-1}; vitreous carbon electrode; potentials are in V vs Fc^+/Fc).

Scheme 3

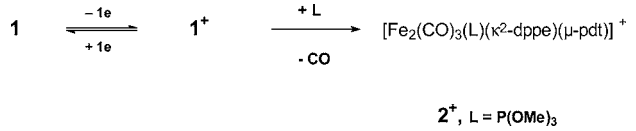

reactions $\mathbf{1}^+ + P(OMe)_3 \rightarrow \mathbf{2}^+ + CO$, and $\mathbf{2}^+ + P(OMe)_3 \rightarrow \mathbf{3}^+ + CO$ (Scheme 4).

As discussed in the previous section, the lowest energy isomer of $\mathbf{1}^+$ corresponds to a rotated structure featuring a vacant coordination site on the Fe(dppe) moiety. The structural features of such an isomer might suggest that $P(OMe)_3$ will bind to the five-coordinated Fe atom where dppe is bound. However, comparative analysis of the transition states for $P(OMe)_3$ binding to $\mathbf{1}^+$ along different reaction channels (see Scheme 5) reveals that the free energy barrier (computed using as reference the lowest energy $\mathbf{1}^+$ isomer) for $P(OMe)_3$ binding to the $Fe(CO)_3$ moiety is 9.9 kcal/mol and, more importantly, 8.7 kcal/mol lower than the corresponding energy barrier for $P(OMe)_3$ binding to the iron atom coordinated by dppe. Therefore, in the initial step the incoming $P(OMe)_3$ ligand reacts with the $Fe(CO)_3$ moiety of $\mathbf{1}^+$. In the intermediate species which is formed (hereafter referred to as **2-CO**$^+$; Scheme 4) one of the terminal CO ligand of the $Fe(CO)_3$ moiety has moved to a bridging position, while the CO group that occupied a bridging position in $\mathbf{1}^+$ has moved to a terminal position.

In the lowest energy **2-CO**$^+$ isomer both iron atoms are six-coordinated, with dibasal dppe and apical $P(OMe)_3$ coordination. Other **2-CO**$^+$ isomers, differing by the relative orientation of dppe and $P(OMe)_3$, are computed to be at least 1.9 kcal/mol higher in energy (see Supporting Information).

Scheme 4. Computed Free Energy Profile[a] **for the Reactions $\mathbf{1}^+ + P(OMe)_3 \rightarrow \mathbf{2}^+ + CO$, and $\mathbf{2}^+ + P(OMe)_3 \rightarrow \mathbf{3}^+ + CO$**[b]

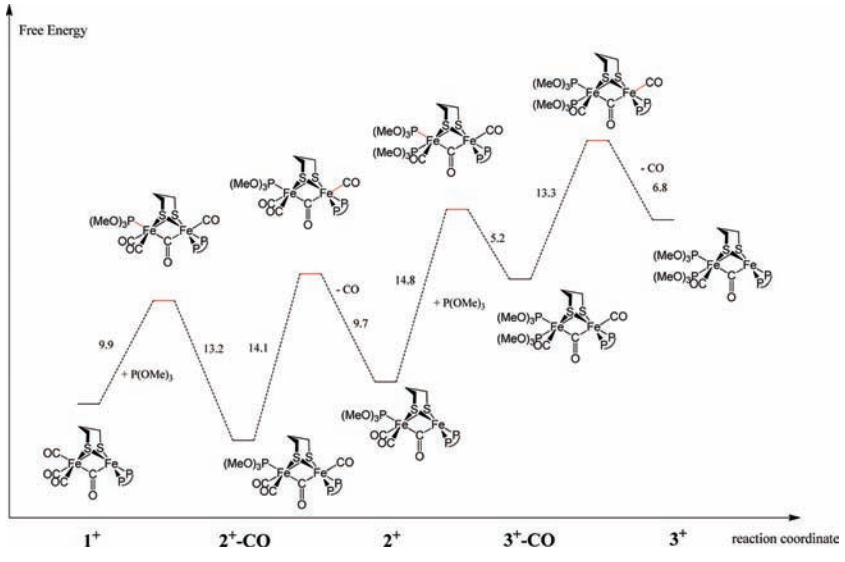

[a]See Reference 48.

[b]Energies in kcal/mol. For the sake of clarity, bonds which are formed or cleaved in transition states are shown in red.

dx.doi.org/10.1021/ic201601q | Inorg. Chem. 2011, 50, 12575–12585

Scheme 5. Relative Energies[a] and Structures of the Transition States for the Reaction between 1^+ and $P(OMe)_3$

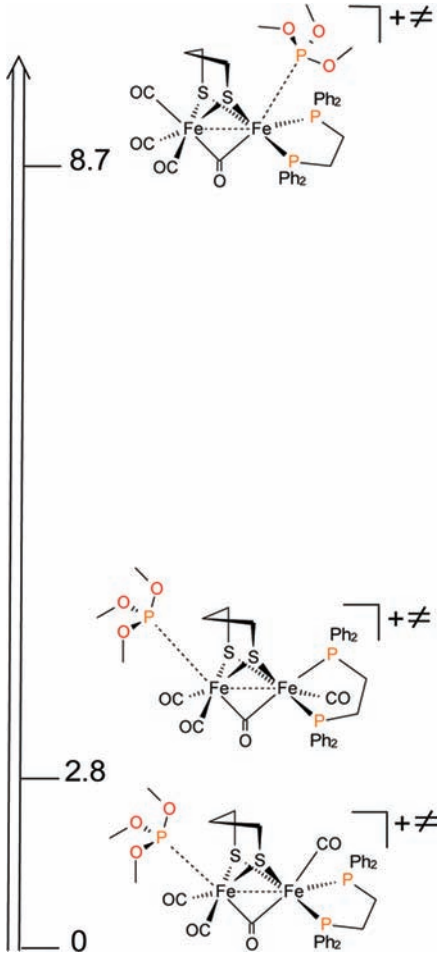

[a]In kcal/mol.

The intermediate species **2-CO**$^+$ can lose a CO ligand forming the rotated species $\mathbf{2}^+$, which features dibasal coordination of the dppe ligand (Figure 7). In fact, sampling

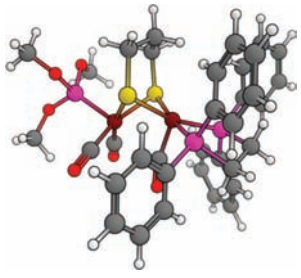

Figure 7. DFT optimized structure of the lowest energy $\mathbf{2}^+$ isomer. For the sake of clarity atoms are shown as follows. Carbon, gray; hydrogen, white; sulfur, yellow; oxygen, red; phosphorus, light purple; iron, dark purple.

of different reaction paths revealed that the lowest free energy barrier route implies CO loss from the iron atom coordinated by dppe ($\Delta G^{\ddagger}$ = 14.1 kcal/mol). Other $\mathbf{2}^+$ isomers lie at least 3.9 kcal/mol higher in energy (see Supporting Information, Scheme S1).

$\mathbf{2}^+$ can then react with a second $P(OMe)_3$ molecule forming **3-CO**$^+$. As observed for the analogous reaction between $\mathbf{1}^+$ and $P(OMe)_3$, the reaction path characterized by the lowest energy barrier does not imply binding of $P(OMe)_3$ to the vacant coordination site of the Fe(dppe) moiety, but reaction of the phosphine ligand at the iron center where the first $P(OMe)_3$ ligand was bound (Scheme 6).

Scheme 6. Relative Energies[a] of the Transition States for the Reaction between 2^+ and $P(OMe)_3$[b]

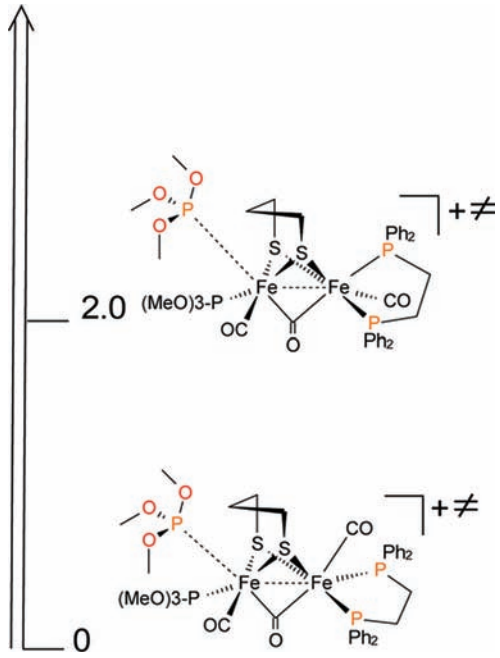

[a]In kcal/mol.

[b]Transition states for the attack of $P(OMe)_3$ to the Fe(dppe) moiety are at least 9 kcal/mol higher in energy, and therefore have not been shown in the scheme.

The energy barrier from the lowest energy $\mathbf{2}^+$ isomer to the transition state leading to **3-CO**$^+$ is 14.8 kcal/mol. In **3-CO**$^+$ the dppe ligand has dibasal coordination, whereas the two $P(OMe)_3$ ligands occupy apical and basal positions. However, it should be noted that several isomers of **3-CO**$^+$, differing for the orientation of the phosphine ligands, are within 1 kcal/mol (data not shown) and therefore might coexist in solution.

CO loss from **3-CO**$^+$, leading to $\mathbf{3}^+$, takes place going through a transition state ($\Delta G^{\ddagger}$ = 13.3 kcal/mol; Scheme 4) in which the CO group is lost from the iron atom coordinated by dppe (Supporting Information, Scheme S2). The lowest energy $\mathbf{3}^+$ isomer is characterized by rotated geometry and a vacant coordination site on the Fe(dppe) moiety. However, an eclipsed $\mathbf{3}^+$ isomer is only 0.4 kcal/mol higher in energy (See Supporting Information, Scheme S3). Considering that such an energy difference is well below the expected accuracy of present DFT methods, both isomers can be simultaneously present in solution.

4. DFT Investigations of the Reactivity of 3 with CO.

To fully complement the experimental results, DFT was also used to analyze the mechanism of the reaction between the Fe(I)Fe(I) neutral species **3** and CO. In the reaction **3** + CO → **2** (Scheme 7) the rate determining step corresponds to CO binding to the Fe(dppe) moiety, and the reaction is predicted to be globally exergonic by −15.9 kcal/mol.

dx.doi.org/10.1021/ic201601q | *Inorg. Chem.* 2011, 50, 12575–12585

Scheme 7. DFT Dissection of the Reaction 3 + CO → 2[a]

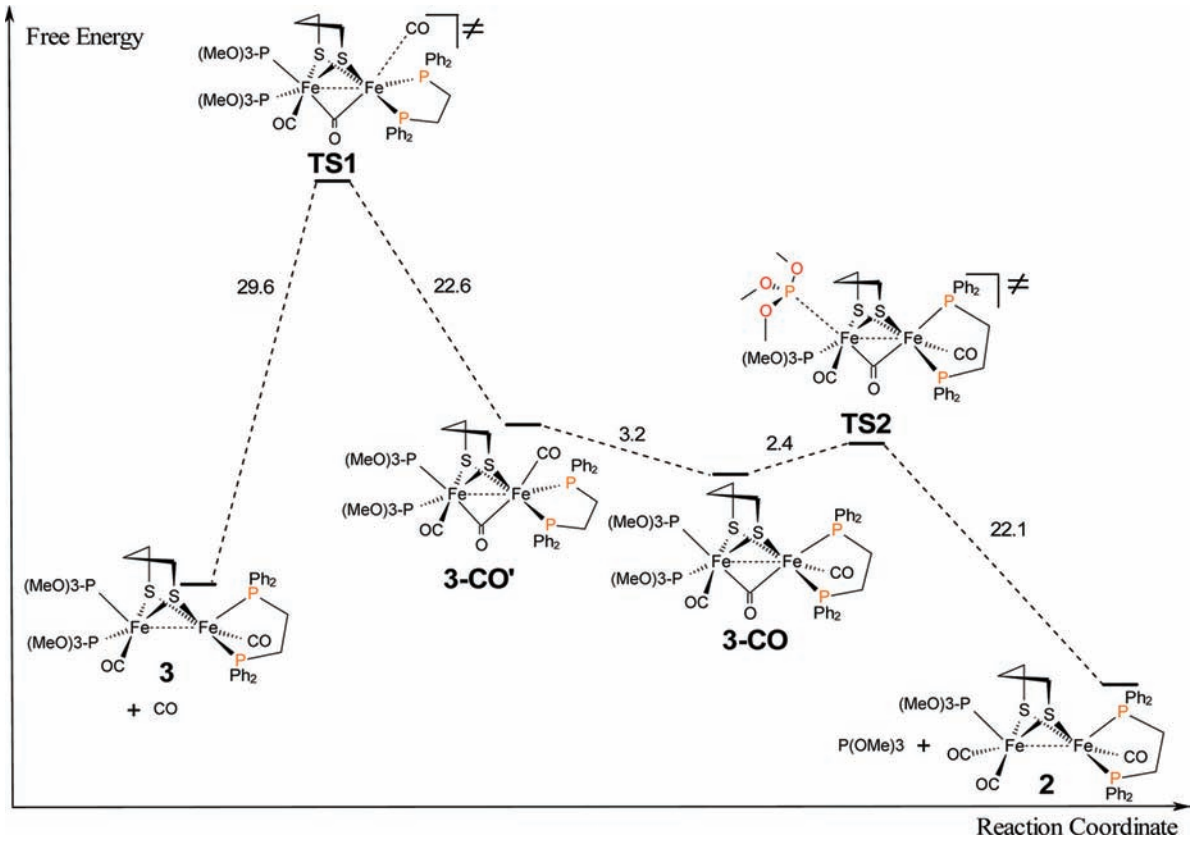

[a]Energy values are in kcal/mol. For the sake of clarity, only the lowest energy isomers of reactants, products, and intermediate species are shown. In addition, the transition state connecting **3-CO**′ and **3-CO** is not shown.

■ DISCUSSION AND CONCLUDING REMARKS

The results reported above underline the enhanced reactivity of complex **1** upon one-electron oxidation, which is entirely consistent with the exposure of a vacant site in the cation. Whether the oxidatively induced structure change occurs in a two-step EC process or in a concerted way could not be firmly established experimentally. However, DFT results favor the former possibility. Electron extraction from **1** initially leads to an eclipsed $\mathbf{1}^+$ isomer, which then spontaneously rearranges to the lowest energy rotated form (Scheme 8). However, it should be noted that the computed energy barriers for the interconversion among $\mathbf{1}^+$ isomers are very low (Berry pseudorotations; energy barriers lower than 6 kcal/mol), indicating that isomerization of $\mathbf{1}^+$ is a very fast process, thus supporting the observation that it can be very difficult to experimentally distinguish between an EC and a QR process in the oxidation of this class of compounds.

Although we could not crystallographically characterize $\mathbf{1}^+$ nor the cationic derivatives resulting from its reactions with $P(OMe)_3$, the presence of a $Fe(CO)_2\{P(OMe)_3\}$ entity in the neutral complex **2** is an indirect evidence for the accessibility of an isomer of $\mathbf{1}^+$ with a rotated $Fe(CO)_3$. This is fully supported by the DFT results. In fact, it turned out that the lowest energy $\mathbf{1}^+$ isomer, which is characterized by a vacant coordination site on the Fe(dppe) moiety, is much less reactive than the corresponding isomer featuring a vacant coordination site on $Fe(CO)_3$. The origin of the different reactivity of the two rotated $\mathbf{1}^+$ isomers is revealed by a comparative analysis of the electronic and steric properties of the five coordinated iron atoms in the two isomers. In fact, while partial atomic charges of both iron atoms are very similar in the two rotated isomers (data not shown), the bulky phenyl groups of dppe strongly hinder the accessibility of the five coordinated iron atom in the lowest energy isomer (see Figure 2).

The interconversion of the $P(OMe)_3$-substituted cations $\mathbf{2}^+$ and $\mathbf{3}^+$ deserves several comments. In the mechanism proposed in the light of the experimental and DFT results, the incoming ligand ($P(OMe)_3$ or CO) pushes the semibridging CO toward the neighboring metal center, which eventually results in the loss of the ligand *trans* to the swinging carbonyl group (Scheme 9). Such a mechanism, that has been reported for neutral or anionic diiron dithiolate complexes,[12,13,49−52] was also recently invoked to account for the incorporation of ^{13}CO at both metal centers of Fe(I)Fe(II) complexes, $[Fe_2(CO)_4(PMe_3)(NHC)(\mu\text{-pdt})]^+$ (NHC = imidazol-2-ylidene ligands), submitted to a ^{13}CO atmosphere.[23]

The reversibility of the processes in Scheme 9 requires that the rotated center in $\mathbf{2}^+$ is not the same as in $\mathbf{3}^+$. Actually, the most stable form of $\mathbf{2}^+$ was shown by DFT to have a rotated Fe(dppe)(CO) center (that is the same as in $\mathbf{3}^+$, Scheme 4). Nevertheless, the reaction of $P(OMe)_3$ with $\mathbf{2}^+$ takes place at the iron center already carrying the first $P(OMe)_3$ ligand (Scheme 6), so that Scheme 9 shows the most reactive, not the most stable, isomer of $\mathbf{2}^+$. This is reminiscent of the results of recent theoretical studies of $[Fe_2(CO)_3(PR_3)(\kappa^2\text{-dppv})(\mu\text{-pdt})]^+$ analogues of $\mathbf{2}^+$ (R = Me or i-Pr) that demonstrated that the identity of the most stable rotated cation was dependent on the R group, and that when R = i-Pr, the

dx.doi.org/10.1021/ic201601q | Inorg. Chem. 2011, 50, 12575−12585

Scheme 8. Schematic Representation of the 1^+ Isomers That Can Be Formed upon One-Electron Oxidation of 1[a]

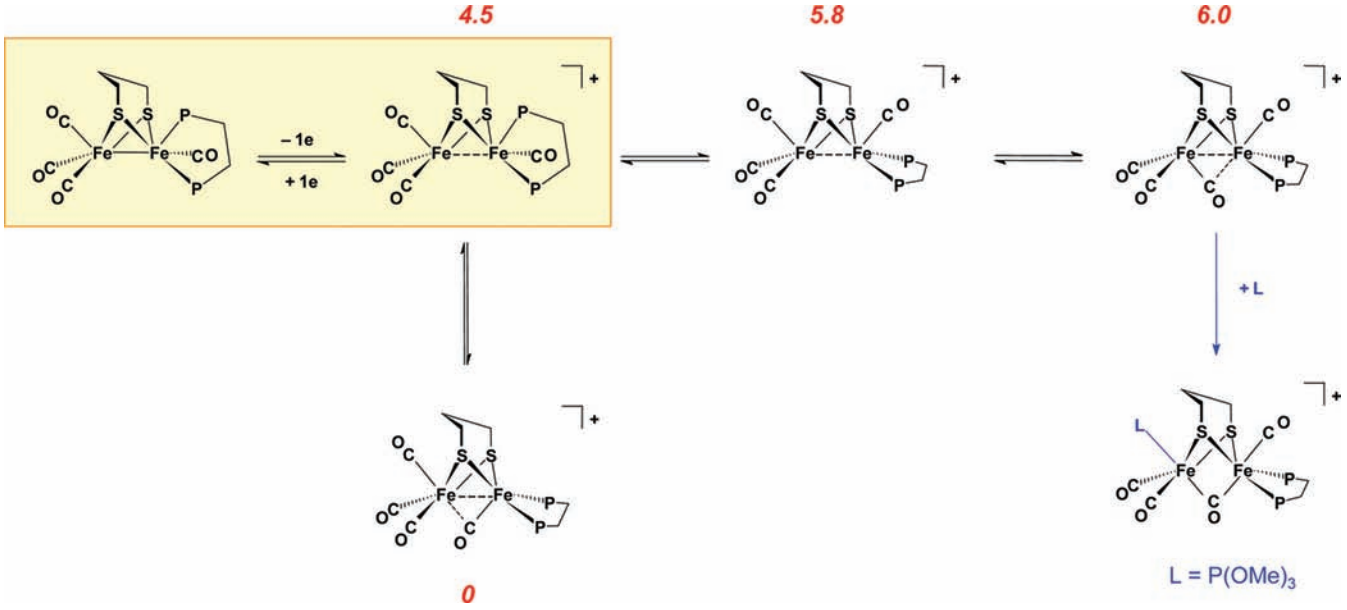

[a]Computed energies (in kcal/mol) of the different 1^+ isomers are relative to the lowest energy form. The reaction pathway between 1^+ and the ligand L = $P(OMe)_3$ characterized by the lowest energy barrier is also shown (in blue).

Scheme 9. Proposed Reaction Sequence for the Interconversion $2^+ \leftrightarrow 3^+$[a]

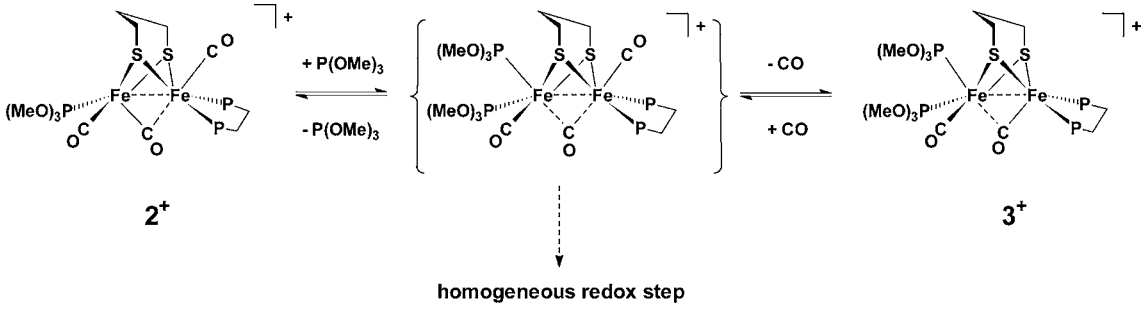

[a]PP = dppe.

rotation of the $Fe(CO)_2(Pi\text{-}Pr_3)$ and of the Fe(CO)(dppv) centers were nearly isoenergetic.[21]

It is also worth noting that the only species detected in the $2^+ \leftrightarrow 3^+$ interconversion are 2^+ and 3^+. The fact that the intermediate in braces (Scheme 9) corresponding to the species **3-CO**$^+$ characterized by DFT calculations, was not detected during the conversion of 2^+ to 3^+ would suggest that the slowest step of the sequence is the binding of $P(OMe)_3$. On the other hand, our results indicate that the reaction of 3^+ with CO involves two types of processes, that is, the replacement of a $P(OMe)_3$ ligand by CO (which produces 2^+) and a minor homogeneous redox reaction. The latter may be a sign of the transient existence of the CO-bridged intermediate. Assuming that the slow step of the $3^+ \rightarrow 2^+$ conversion is the loss of the $P(OMe)_3$ ligand, the intermediate may be sufficiently long-lived, as suggested by our DFT results, to undergo competing reactions, that is, homogeneous electron transfer and ligand loss, when it is formed by reaction of 3^+ with CO (Scheme 9).

As for the corresponding **3** → **2** conversion, DFT results highlight that the process is thermodynamically favored, in good agreement with the experimentally observed quantitative production of **2** starting from **3**. In addition, it is worth noting that both Fe(I)Fe(I) and Fe(I)Fe(II) species, even if differing for the ground state geometry of reactants (eclipsed and rotated for Fe(I)Fe(I) and Fe(I)Fe(II) species, respectively), as well as for the formal oxidation state of the iron atom which interacts with the incoming ligand, proceeds via a very similar mechanism.

EXPERIMENTAL SECTION

Methods and Materials. All the experiments were carried out under an inert atmosphere, using Schlenk techniques for the syntheses. Dichloromethane was predried using conventional methods and distilled prior to use. The diiron complex $[Fe_2(CO)_4(\kappa^2\text{-dppe})(\mu\text{-pdt})]$ **1** was prepared according to reported methods.[14a]

The preparation and the purification of the supporting electrolyte $[NBu_4][PF_6]$ were as described previously.[53] The electrochemical equipment consisted of a PGSTAT 12 or a μ-AUTOLAB (Type III) driven by the GPES software. A GCU potentiostat and a IG5-N integrator (Tacussel/Radiometer) were used for controlled-potential electrolyses and coulometry. All the potentials (text, figures) are referred to the ferrocene-ferrocenium couple; ferrocene was added as an internal standard at the end of the experiments.

^1H, $^{31}P\text{-}\{^1H\}$ NMR spectra were recorded on a Bruker AMX 400 and AC300 spectrometer and were referenced to $SiMe_4$ (^1H) and H_3PO_4 (^{31}P). VT NMR experiments were carried out on a Bruker DRX 500 spectrometer. The infrared spectra were recorded on a Nicolet Nexus Fourier transform spectrometer. Chemical analyses

dx.doi.org/10.1021/ic201601q | Inorg. Chem. 2011, 50, 12575–12585

were made by the Service de Microanalyses I.C.N.S., Gif sur Yvette, France. Crystal data (Table 2) for compound **2** were collected on a Oxford Diffraction X-calibur-2 CCD diffractometer, equipped with a jet cooler device and graphite-monochromated Mo Kα radiation (λ = 0.71073 Å). The structures were solved and refined by standard procedures.[54−56]

Table 2. Crystallographic Data for Complex 2·CH_2Cl_2, C_6H_{14}

	2·CH_2Cl_2, C_6H_{14}
empirical formula	$C_{42}H_{55}Cl_2Fe_2O_6P_3S_2$
formula weight	995.49
temperature/K	170(2)
crystal system	monoclinic
space group	$P21/n$
a (Å)	16.9360(9)
b (Å)	10.7232(5)
c (Å)	25.4174(13)
α (deg)	
β (deg)	93.334(4)
γ (deg)	
V (Å^3)	4608.2(4)
Z	4
ρ_{calc} (Mg mm^{-3})	1.435
μ (mm^{-1})	0.985
crystal size (mm)	0.23 × 0.07 × 0.03
range of θ (deg)	2.80−25.35
reflections measured	31636
R_{int}	0.1164
unique data/parameters	8405/508
R_1 ($I > 2\sigma(I)$)	0.0759
R_1 (all data)	0.1469
wR_2 (all data)	0.1829
goodness of-fit on F^2	1.060
$\Delta\rho_{max}$, $\Delta\rho_{min}$/e Å^{-3}	1.389, −0.395

Digital Simulations. All the simulations were performed with DigiElch Special Build Version 3 (Build SB3.600).[38] Details of the procedure are given as Supporting Information.

Electrosynthesis of $[Fe_2(CO)_2\{P(OMe)_3\}_2(\kappa^2\text{-dppe})(\mu\text{-pdt})]^{+/0}$ ($3^{+/0}$). In a typical experiment, 23.4 mg (3.21 mmol) of **1** and 11.4 μL of $P(OMe)_3$ (9.67 mmol, 3 equiv) were dissolved in 20 mL of CH_2Cl_2-$[NBu_4][PF_6]$ at room temperature in the electrochemical cell. The controlled-potential oxidation, carried out at −0.18 V (graphite anode), was terminated after the passage of 0.93 F mol^{-1} **1**. The CV of the electrolyzed solution showed that $\mathbf{3}^+$, characterized by a reversible reduction at −0.88 V and an irreversible oxidation at 0.14 V, was formed in 92% yield.[40]

The solution of $\mathbf{3}^+$ was submitted to a controlled-potential reduction at −0.96 V (graphite cathode). The current decayed to the background level after the passage of 0.94 F mol^{-1} of the initial **1**. CV of the catholyte showed that $\mathbf{3}^+$ had been converted essentially quantitatively to the neutral complex **3** (typical yield: 90%).[40] The solution of **3** was canulated in a Schlenk flask under N_2, and the solvent evaporated under vacuum. The residue was extracted by diethyl ether (3 × 20 mL). After evaporation of the solvent, the solid residue was dried under vacuum.

3. IR (CH_2Cl_2, cm^{-1}): ν(CO) 1899 (s), 1880 (s). ^{31}P-{^{1}H} NMR ($CDCl_3$, 25 °C), δ: 177.5 $P(OMe)_3$), 85.4 (dppe). No satisfactory elemental analysis could be obtained for **3**, because of the limited stability of the complex.

Synthesis of $[Fe_2(CO)_3\{P(OMe)_3\}(\kappa^2\text{-dppe})(\mu\text{-pdt})]$ (2). **2** was obtained by bubbling CO for a few minutes in a CH_2Cl_2-$[NBu_4][PF_6]$ solution of **3** obtained as described above. The solution of **2** was canulated from the electrochemical cell in a Schlenk flask under N_2, and the solvent was then removed under vacuum. **2** was extracted with diethyl ether (3 × 20 mL). Evaporation of the solvent gave **2** as a brown solid. Single crystals of **2** were obtained from a hexane-dichloromethane (1:1) solution at −18 °C.

2. IR (CH_2Cl_2, cm^{-1}): ν(CO) 1968(s), 1913(s) and 1892(sh). ^{1}H NMR ($CDCl_3$, 25 °C), δ: 7.94−7.40 (m, 20H, C_6H_5), 3.74 (d, 9H, J = 11.2 Hz, $P(OCH_3)_3$), 2.64 (m, 4H, P-CH_2−CH_2−P), 1.59 (m, 4H, $S(CH_2)_3S$), 1.38 (m, 1H, $S(CH_2)_3S$), 0.92 (m, 1H, $S(CH_2)_3S$). ^{31}P-{^{1}H} NMR ($CDCl_3$, 25 °C), δ: 179.7 ($P(OMe)_3$), 89.4 (dppe). Anal. Calcd (%) for $C_{35}H_{39}Fe_2O_6P_3S_2$: C, 50.99; H, 4.77. Found: C, 50.23; H, 4.73.

DFT Calculations. DFT calculations have been performed by using the TURBOMOLE suite of programs,[57] at the B-P86/TZVP[58,59] level of theory, which is well suited for studying [FeFe]-hydrogenase models.[60−62]

First-order saddle and minimum points on the potential energy surface (PES) have been determined by means of energy gradient techniques, and a full vibrational analysis has been carried out to further characterize each stationary point. The optimization of transition state structures has been performed according to a procedure based on a pseudo-Newton−Raphson method. First, geometry optimization of a guess transition state structure is carried out by constraining the distance corresponding to the reaction coordinate (RC). After performing the vibrational analysis of the constrained minimum energy structures, the negative eigenmode associated to the RC is followed to locate the true transition state structure, that is, the maximum energy point along the trajectory which joins two adjacent minima.

Free energy (G) values have been obtained from the electronic SCF energy considering three contributions to the total partition function (Q), namely, $q_{translational}$, $q_{rotational}$, $q_{vibrational}$, under the approximation that Q may be written as the product of such terms. Evaluation of H and S contributions has been made by setting T and P values tot 298.15 K and 1 bar, respectively.

An implicit treatment of solvent effect (COSMO,[63] ε = 9.1, dichloromethane) has been employed.

In light of available experimental data and considering the chemical nature of the ligands, only low-spin species have been investigated.

■ ASSOCIATED CONTENT

Supporting Information

Crystallographic data in CIF format. Further details are given in Figures S1−S9, Schemes S1−S3, and Tables S1−S2. This material is available free of charge via the Internet at http://pubs.acs.org.

■ AUTHOR INFORMATION

Corresponding Author

*E-mail: jean.talarmin@univ-brest.fr (J.T.), philippe.schollhammer@univ-brest.fr (P.S.), luca.degioia@unimib.it (L.D.G.).

■ ACKNOWLEDGMENTS

CNRS (Centre National de la Recherche Scientifique), ANR (Programme "PhotoBioH2" and "CatH2"), Université de Bretagne Occidentale and University of Milano-Bicocca are acknowledged for financial support. We are grateful to Dr. F. Michaud for the crystallographic measurements of $\mathbf{4}[\mathbf{PF_6}]_2$ and to N. Kervarec for recording the VT ^{1}H and ^{31}P{^{1}H} NMR spectra. D.C. is grateful to the Ministère de l'Education Nationale, de l'Enseignement Supérieur et de la Recherche for providing a studentship.

■ REFERENCES

(1) (a) Peters, J. W.; Lanzilotta, W. N.; Lemon, B. J.; Seefeldt, L. C. *Science* **1998**, *282*, 1853−1858. (b) Lemon, B. J.; Peters, J. W. *Biochemistry* **1999**, *38*, 12969−12973.

(2) (a) Nicolet, Y.; Piras, C.; Legrand, P.; Hatchikian, C. E.; Fontecilla-Camps, J. C. *Structure* **1999**, *7*, 13−23. (b) Nicolet, Y.; de Lacey, A. L.; Vernede, X.; Fernandez, V. M.; Hatchikian, C. E.; Fontecilla-Camps, J. C. *J. Am. Chem. Soc.* **2001**, *123*, 1596−1602.
(3) For recent reviews on the hydrogenases enzymes, see: (a) Fontecilla-Camps, J. C.; Volbeda, A.; Cavazza, C.; Nicolet, Y. *Chem. Rev.* **2007**, *107*, 4273−4303. (b) de Lacey, A. L.; Fernandez, V. M.; Rousset, M.; Cammack, R. *Chem. Rev.* **2007**, *107*, 4304−4330. (c) Lubitz, W.; Reijerse, E.; van Gastel, M. *Chem. Rev.* **2007**, *107*, 4331−4365. (d) Vincent, K. A.; Parkin, A.; Armstrong, F. A. *Chem. Rev.* **2007**, *107*, 4366−4413. (e) Armstrong, F. A. *Curr. Opin. Chem. Biol.* **2004**, *8*, 133−140. Frey, M. *ChemBioChem* **2002**, *3*, 153−160.
(4) For recent reviews on models of the hydrogenases enzymes, see: (a) Gloaguen, F.; Rauchfuss, T. B. *Chem. Soc. Rev.* **2009**, *38*, 100−108. (b) Capon, J.-F.; Gloaguen, F.; Pétillon, F. Y.; Schollhammer, P.; Talarmin, J. *Coord. Chem. Rev.* **2009**, *253*, 1476−1494. (c) Tard, C.; Pickett, C. J. *Chem. Rev.* **2009**, *109*, 2245−2274. (d) Felton, G. A. N.; Mebi, C. A.; Petro, B. J.; Vannucci, A. K.; Evans, D. H.; Glass, R. S.; Lichtenberger, D. L. *J. Organomet. Chem.* **2009**, *694*, 2681−2699. (e) Heinekey, D. M. *J. Organomet. Chem.* **2009**, *694*, 2671−2680. (f) Best, S. P.; Cheah, M. H. *Radiat. Phys. Chem.* **2010**, *79*, 185−194.
(5) van der Vlugt, J. I.; Rauchfuss, T. B.; Whaley, C. M.; Wilson, S. R. *J. Am. Chem. Soc.* **2005**, *127*, 16012−16013.
(6) (a) Cao, Z.; Hall, M. B. *J. Am. Chem. Soc.* **2001**, *123*, 3734−3742. (b) Fan, H.-F.; Hall, M. B. *J. Am. Chem. Soc.* **2001**, *123*, 3828−3829.
(7) (a) Liu, Z. P.; Hu, P. *J. Am. Chem. Soc.* **2002**, *124*, 5175−5182. (b) Liu, Z.-P.; Hu, P. *J. Chem. Phys.* **2002**, *117*, 8177−8180.
(8) (a) Greco, C.; Bruschi, M.; De Gioia, L.; Ryde, U. *Inorg. Chem.* **2007**, *46*, 5911−5921. (b) Bruschi, M.; Greco, C.; Fantucci, P.; De Gioia, L. *Inorg. Chem.* **2008**, *47*, 6056−6071.
(9) Tye, J. W.; Darensbourg, M. Y.; Hall, M. B. *Inorg. Chem.* **2006**, *45*, 1552−1569. Bruschi, M.; Fantucci, P.; De Gioia, L. *Inorg. Chem.* **2004**, *43*, 3733−3741.
(10) (a) Adam, F. I.; Hogarth, G.; Richards, I.; Sanchez, B. E. *Dalton Trans.* **2007**, 2495−2498. (b) Adam, F. I.; Hogarth, G.; Richards, I. *J. Organomet. Chem.* **2007**, *692*, 3957−3968. (c) Hogarth, G.; Richards, I. *Inorg. Chem. Commun.* **2007**, *10*, 66−70. (d) Adam, F. I.; Hogarth, G.; Kabir, S. E.; Richards, I. *C. R. Chim.* **2008**, *11*, 890−905.
(11) (a) Duan, L.; Wang, M.; Li, P.; Na, Y.; Wang, N.; Sun, L. *Dalton Trans.* **2007**, 1277−1283. (b) Wang, N.; Zhang, T.; Li, P.; Liu, J.; Sun, L. *Chem. Commun.* **2008**, 5800−5802. (c) Wang, N.; Wang, M.; Liu, J.; Jin, K.; Chen, L.; Sun, L. *Inorg. Chem.* **2009**, *48*, 11551−11558.
(12) Wang, N.; Wang, M.; Liu, T.; Li, P.; Zhang, T.; Darensbourg, M. Y.; Sun, L. *Inorg. Chem.* **2008**, *47*, 6948−6955.
(13) Justice, A. K.; Zampella, G.; De Gioia, L.; Rauchfuss, T. B.; van der Vlugt, J. I.; Wilson, S. R. *Inorg. Chem.* **2007**, *46*, 1655−1664.
(14) (a) Ezzaher, S.; Capon, J.-F.; Gloaguen, F.; Pétillon, F. Y.; Schollhammer, P.; Talarmin, J.; Pichon, R.; Kervarec, N. *Inorg. Chem.* **2007**, *46*, 3426−3428. (b) Morvan, D.; Capon, J.-F.; Gloaguen, F.; Le Goff, A.; Marchivie, M.; Michaud, F.; Schollhammer, P.; Talarmin, J.; Yaouanc, J.-J.; Pichon, R.; Kervarec, N. *Organometallics* **2007**, *26*, 2042−2052. (c) Orain, P.-Y.; Capon, J.-F.; Kervarec, N.; Gloaguen, F.; Pétillon, F. Y.; Pichon, R.; Schollhammer, P.; Talarmin, J. *Dalton Trans.* **2007**, 3754−3756. (d) Ezzaher, S.; Capon, J.-F.; Gloaguen, F.; Kervarec, N.; Pétillon, F. Y.; Pichon, R.; Schollhammer, P.; Talarmin, J. *C. R. Chim.* **2008**, *11*, 906−914. (e) Morvan, D.; Capon, J.-F.; Gloaguen, F.; Pétillon, F. Y.; Schollhammer, P.; Talarmin, J.; Yaouanc, J.-J.; Michaud, F.; Kervarec, N. *J. Organomet. Chem.* **2009**, *694*, 2801−2807.
(15) Song, L.-C.; Yang, Z.-Y.; Bian, H.-Z.; Liu, Y.; Wang, H.-T.; Liu, X.-F.; Hu, Q.-M. *Organometallics* **2005**, *24*, 6126−6135.
(16) (a) Lemon, B. J.; Peters, J. W. *Biochemistry* **1999**, *38*, 12969−12973. (b) Bennett, B.; Lemon, B. J.; Peters, J. W. *Biochemistry* **2000**, *39*, 7455−7460. (c) Lemon, B. J.; Peters, J. W. *J. Am. Chem. Soc.* **2000**, *122*, 3793−3794. (d) Chen, Z.; Lemon, B. J.; Huang, S.; Swartz, D. J.; Peters, J. W.; Bagley, K. A. *Biochemistry* **2002**, *41*, 2036−2043.
(17) Razavet, M.; Borg, S. J.; George, S. J.; Best, S. P.; Fairhurst, S. A.; Pickett, C. J. *Chem. Commun.* **2002**, 700−701.
(18) Liu, T.; Darensbourg, M. Y. *J. Am. Chem. Soc.* **2007**, *129*, 7008−7009.
(19) Justice, A. K.; Rauchfuss, T. B.; Wilson, S. R. *Angew. Chem., Int. Ed.* **2007**, *46*, 6152−6154.
(20) Singleton, M. L.; Bhuvanesh, N.; Reibenspies, J. H.; Darensbourg, M. Y. *Angew. Chem., Int. Ed.* **2008**, *47*, 9492−9495.
(21) Justice, A. K.; De Gioia, L.; Nilges, M. J.; Rauchfuss, T. B.; Wilson, S. R.; Zampella, G. *Inorg. Chem.* **2008**, *47*, 7405−7414.
(22) Justice, A. K.; Nilges, M. J.; Rauchfuss, T. B.; Wilson, S. R.; De Gioia, L.; Zampella, G. *J. Am. Chem. Soc.* **2008**, *130*, 5293−5301.
(23) Thomas, C. M.; Liu, T.; Hall, M. B.; Darensbourg, M. Y. *Inorg. Chem.* **2008**, *47*, 7009−7024.
(24) Thomas, C. M.; Liu, T.; Hall, M. B.; Darensbourg, M. Y. *Chem. Commun.* **2008**, 1563−1565.
(25) Thomas, C. M.; Darensbourg, M. Y.; Hall, M. B. *J. Inorg. Biochem.* **2007**, *101*, 1752−1757.
(26) Evans, D. H. *Chem. Rev.* **2008**, *108*, 2113−2144.
(27) Macias-Ruvalcaba, N. A.; Evans, D. H. *Chem.—Eur. J.* **2007**, *13*, 4386−4395.
(28) Evans, D. H.; O'Connell, K. M. In *Electroanalytical Chemistry*; Bard, A. J., Ed., Marcel Dekker: New York, 1986; Vol. *14*, pp 113−207.
(29) Geiger, W. E. *Organometallics* **2007**, *26*, 5738−5765.
(30) Geiger, W. E. In *Progress in Inorganic Chemistry*; Lippard, S. J., Ed.; John Wiley & Sons: New York, 1985; Vol. *33*, pp 275−352.
(31) Bond, A. M.; Colton, R. *Coord. Chem. Rev.* **1997**, *166*, 161−180.
(32) Pombeiro, A. J. L.; Guedes da Silva, M. F. C.; Lemos, M. A. N. D. A. *Coord. Chem. Rev.* **2001**, *219−221*, 53−80.
(33) The parameters i_p and E_p are respectively the peak current and the peak potential of a redox process; $E_{1/2} = (E_p^a + E_p^c)/2$; E_p^a, i_p^a and E_p^c, i_p^c are respectively the potential and the current of the anodic and of the cathodic peak of a reversible process; $\Delta E_p = E_p^a - E_p^c$. The scan rate in CV experiments is v (V s^{-1}). An ECE process consists of a chemical reaction (C) comprised between two electron transfer steps (E).
(34) (a) The deduction of the number of electrons involved in the oxidation of **1** is made by comparison of the current functions for equimolar solutions of **1** and of $(Fe_2(CO)_4(\kappa^2\text{-dppe})(\mu\text{-pdt})(\mu\text{-H}))^+$ (one-electron oxidation)[34b] at different scan rates. This method is valid if the complexes have identical diffusion coefficients, which is a reasonable assumption owing to their similar size and structure. (b) Ezzaher, S.; Capon, J.-F.; Dumontet, N.; Gloaguen, F.; Pétillon, F. Y.; Schollhammer, P.; Talarmin, J. *J. Electroanal. Chem.* **2009**, *626*, 161−170.
(35) (a) Petro, B. J.; Vannucci, A. K.; Lockett, L. T.; Mebi, C.; Kottani, R.; Gruhn, N. E.; Nichol, G. S.; Goodyer, P. A.; Evans, D. H.; Glass, R. S.; Lichtenberger, D. L. *J. Mol. Struct.* **2008**, *890*, 281−288. (b) Felton, G. A. N.; Vannucci, A. K.; Chen, J.; Lockett, L. T.; Okumura, N.; Petro, B. J.; Zakai, U. I.; Evans, D. H.; Glass, R. S.; Lichtenberger, D. L. *J. Am. Chem. Soc.* **2007**, *129*, 12521−12530.
(36) Geiger, W. E.; Camire Ohrenberg, N. C.; Yeomans, B.; Connelly, N. G.; Emslie, D. J. H. *J. Am. Chem. Soc.* **2003**, *125*, 8680−8688.
(37) (a) The peak separation, ΔE_p, was measured at a clean electrode surface for 0.05 V $s^{-1} \leq v \leq 10$ V s^{-1}. However, values of ΔE_p at slow scan rates (0.05 V $s^{-1} \leq v \leq 0.4$ V s^{-1}) were selected to minimize the effects of uncompensated solution resistance. The apparent hetero geneous electron transfer rate constant calculated according to ref. 37b was $k_s^{app} = 0.005 \pm 0.001$ cm s^{-1}. (b) Nicholson, R. S. *Anal. Chem.* **1965**, *37*, 1351−1355.
(38) For detailed information concerning DigiElch, see: (a) Rudolph, M. *J. Electroanal. Chem.* **2003**, *543*, 23−29. (b) Rudolph, M. *J. Electroanal. Chem.* **2004**, *571*, 289−307. (c) Rudolph, M. *J. Comput. Chem.* **2005**, *26*, 619−632. (d) Rudolph, M. *J. Comput. Chem.* **2005**, *26*, 633−641. (e) Rudolph, M. *J. Comput. Chem.* **2005**, *26*, 1193−1204.
(39) (a) Bard, A. J.; Faulkner, L. R. In *Electrochemical Methods. Fundamentals and Applications*; Wiley: New York, 1980; Chapter 11, pp 429−485. (b) Savéant, J.-M. In *Elements of Molecular and Biomolecular Electrochemistry - An Electrochemical Approach to Electron Transfer Chemistry*; Wiley: New York, 2006; Chapter 2, pp 78−181.

(40) The product yields of the controlled-potential oxidations were estimated from the comparison of the oxidation peak current of **1** in the absence of substrate, to the reduction peak current of the electrogenerated cation, assuming identical diffusion coefficients. Similarly, the yields of the controlled-potential reductions were estimated by comparison of the peak current of the cation to that of the neutral product formed by electrolysis.
(41) Justice, A. K.; Zampella, G.; De Gioia, L.; Rauchfuss, T. B. *Chem. Commun.* **2007**, 2019−2021.
(42) Morvan, D.; Capon, J.-F.; Gloaguen, F.; Schollhammer, P.; Talarmin, J. *Eur. J. Inorg. Chem.* **2007**, 5062−5068.
(43) Capon, J.-F.; Gloaguen, F.; Pétillon, F. Y.; Schollhammer, P.; Talarmin, J. *Eur. J. Inorg. Chem.* **2008**, 4671−4681.
(44) Justice, A. K.; Zampella, G.; De Gioia, L.; Rauchfuss, T. B.; van der Vlugt, J. I.; Wilson, S. R. *Inorg. Chem.* **2007**, *46*, 1655−1664.
(45) Orain, P. Y.; Capon, J.-F.; Gloaguen, F.; Pétillon, F. Y.; Schollhammer, P.; Talarmin, J.; Zampella, G.; De Gioia, L.; Roisnel, T. *Inorg. Chem.* **2010**, *49*, 5003−5008.
(46) Wang, N.; Wang, M.; Liu, T.; Li, P.; Zhang, T.; Darensbourg, M. Y.; Sun, L. *Inorg. Chem.* **2008**, *47*, 6948−6955.
(47) Barton, B.; Zampella, G.; Justice, A. K.; De Gioia, L.; Rauchfuss, T. B.; Wilson, S. R. *Dalton Trans.* **2010**, 3011−3019.
(48) The scheme has been conceived to show relative energy data concerning relevant stationary points of the PES associated to the reaction pathway going from $\mathbf{1}^+$ to $\mathbf{3}^+$. In fact, steps 1 and 3 in Scheme 4 do not necessarily correspond to actual elementary reaction acts, since possible unimolecular rearrangements have not been explicitly shown in this scheme. For example $\mathbf{1}^+$ might rearrange so as to expose a vacant coordination site on the $Fe(CO)_3$ moiety, before L attack to such site.
(49) S. Ezzaher, S.; Capon, J.-F.; Gloaguen, F.; Pétillon, F. Y.; Schollhammer, P.; Talarmin, J. *Inorg. Chem.* **2007**, *46*, 9863−9872.
(50) George, S. J.; Cui, Z.; Razavet, M.; Pickett, C. J. *Chem.—Eur. J.* **2002**, *8*, 4037−4046.
(51) Zampella, G.; Bruschi, M.; Fantucci, P.; Razavet, M.; Pickett, C. J.; De Gioia, L. *Chem.—Eur. J.* **2005**, *11*, 509−520.
(52) Daraosheh, A. Q.; Harb, M. K.; Windhager, J.; Görls, H.; El-khateeb, M.; Weigand, W. *Organometallics* **2009**, *28*, 6275−6280.
(53) Capon, J.-F.; Ezzaher, S.; Gloaguen, F.; Pétillon, F. Y.; Schollhammer, P.; Talarmin, J.; Davin, T. J.; McGrady, J. E.; Muir, K. W. *New J. Chem.* **2007**, *31*, 2052−2064.
(54) Sheldrick, G. M. *Acta Crystallogr., Sect. A* **2008**, *64*, 112−122.
(55) Altomare, A.; Cascarano, G.; Giacovazzo, C.; Guagliardi, A. *J. Appl. Crystallogr.* **1993**, *26*, 343−350.
(56) Farrugia, L. J. *J. Appl. Crystallogr.* **1999**, *32*, 837−838.
(57) Ahlrichs, R.; Bar, M.; Haser, M.; Horn, H.; Kolmel, C. *Chem. Phys. Lett.* **1989**, *162*, 165−169.
(58) Becke, A. D. *Phys. Rev. A* **1988**, *38*, 3098−3100.
(59) Perdew, J. P. *Phys. Rev. B: Condens. Matter* **1986**, *33*, 8822−8824.
(60) Bertini, L.; Bruschi, M.; De Gioia, L.; Fantucci, P.; Greco, C.; Zampella, G. In *Atomistic Approaches in Modern Biology: From Quantum Chemistry to Molecular Simulations*; Reiher, M., Ed.; Springer: Berlin, Germany, 2007; Vol. *268*, pp 146.
(61) Bruschi, M.; Zampella, G.; Fantucci, P.; De Gioia, L. *Coord. Chem. Rev.* **2005**, *249*, 1620−1640.
(62) Zampella, G.; Greco, C.; Fantucci, P.; De Gioia, L. *Inorg. Chem.* **2006**, *45* (10), 4109−4118.
(63) Schafer, A.; Klamt, A.; Sattel, D.; Lohrenz, J. C. W.; Eckert, F. *Phys. Chem. Chem. Phys.* **2000**, *2*, 2187−2193.